

Differential cross sections for electron-impact excitation of krypton at low incident energies: I. Excitation of the $4p^55s$ configuration

Xuezhe Guo[†], D F Mathews[†], G Mikaelian[†], M A Khakoo[†], A Crowe[‡],
I Kanik[§], S Trajmar[§], V Zeman^{||}*, K Bartschat[¶] and C J Fontes[¶]

[†] Department of Physics, California State University, Fullerton, CA 92834, USA

[‡] Department of Physics, University of Newcastle, Newcastle-upon-Tyne, NE1 7RU, UK

[§] Jet Propulsion Laboratory, California Institute of Technology, Pasadena CA 91109, USA

^{||} Department of Physics and Astronomy, Drake University, Des Moines IA 50311, USA

[¶] Applied Theoretical and Computational Physics Division, Los Alamos National Laboratory, Los Alamos NM 87545, USA

Received 6 November 1999, in final form 7 April 2000

Abstract. The electron-impact excitation of the individual levels that constitute the $4p^55s$ configuration of Kr is experimentally and theoretically investigated at incident electron energies of 20.0, 15.0, 13.5 and 12.0 eV, for scattering angles ranging from 10° to 135° . High resolution electron energy-loss spectroscopy is used to obtain spectral intensities for the excitation of each of the four $4p^55s$ levels from the ground state. The intensities lead to three differential cross section ratios. Absolute electron-impact excitation cross sections are then determined by normalization to elastic scattering cross sections using the conventional inelastic to elastic normalization method. The present theoretical cross sections are calculated using two different methods, namely the R-matrix method and the unitarized first-order many-body theory. Comparisons between the experimental and the theoretical results show some good agreement, but reveal areas where significant improvement of the present models is needed. Additionally, it is shown that in the present case, just as in general for the rare gases, differential cross section ratios provide a sensitive test of theoretical models as well as unique insights concerning relativistic effects in the scattering process. Comparisons with existing models and other experimental data are also presented.

1. Introduction

Electron-impact excitation of heavy rare gases continues to attract great interest in collision physics for several reasons. Rare gases are used in plasma diagnostics for tokamak fusion research (Tawara and Phaneuf 1988), in plasma and laser physics (Rhodes 1983), plasma display panel technology (Williamson *et al* 1994, Veerasingham *et al* 1995) etc. Recent advances in computer technology have enabled large electron-scattering codes to be executable, resulting in more accurate models for electron-impact excitation of LS -coupled target atoms. As an example, we point to the success of the recent convergent close-coupling (CCC) method of Bray and Stelbovics (1992) and Bray (1994) in getting very good agreement with a range of measurements in electron scattering from targets such as K (Stockman *et al* 1999), Na (McClelland *et al* 1989, Scholten *et al* 1993, Allen *et al* 1987) and most recently Ba (Trajmar

* Present address: Department of Clinical Physics, Princess Margaret Hospital, 610 University Ave., Toronto, Ontario, M5G 2M9, Canada.

et al 1999). However, relativistic interactions such as spin-orbit coupling, which are generally important in heavy targets, have yet to be incorporated into the CCC method as it stands today. A similar problem faces the newly developed R-matrix with pseudostates method (RMPS, Bartschat *et al* 1996, Bartschat 1998) which has reproduced many of the results of the CCC. The RMPS also suffers from very large computational demands as the number of coupled channels increases. However, presently there exists the standard semi-relativistic R-matrix code (RM) of Berrington *et al* (1995). This handles the most important effects through the one-electron terms of the Breit-Pauli Hamiltonian. Recently the RM was moderately successful in predicting the polarization of light emitted after electron-impact excitation of Xe by spin-polarized electrons in the near-threshold regime (Zeman *et al* 1998a). This suggests a starting point for more detailed tests of this code especially for angle-differential variables. Using this code, we have performed 5-state (RM5), 15-state (RM15) and 31-state (RM31) calculations in order to assess the convergence of the close-coupling expansion with the number of states, to examine the need (or lack thereof) for a full RMPS calculation. This is motivated by the observation that the theoretical R-matrix approach of Nakazaki *et al* (1997) also provided improved qualitative agreement with recent Xe differential cross section (DCS) measurements at lower energies. These absolute differential cross section measurements (Khakoo *et al* 1996a, b) involved the electron-impact excitation of the lowest four excited configurations ($5p^56s$, $5p^56p$, $5p^55d$ and $5p^57s$) of Xe. The article incorporated results from two perturbative models, i.e. the unitarized distorted-wave approximation (UDWA) and the unitarized first-order many-body theory (UFOMBT). Some of these UFOMBT results were greatly improved over previous calculations due to inclusion of configuration interaction from the $5p^55d$ configuration as explained in Fontes (1998). However, all models available at present mostly show qualitative agreement with experiment.

An additional model, the relativistic distorted-wave approximation (RDWA) of Zuo *et al* (1992) which uses single-electron configuration wavefunctions, focuses on the relativistic terms in the electron-target Hamiltonian using solutions to the Dirac-Fock equation. Recent Kr inelastic electron scattering DCS calculations, using the RDWA, were published by Kaur *et al* (1998). The energy range of perturbative models is limited to the intermediate/high energies and it is of interest to develop these models for lower incident energies (30 eV or below) where cross sections are larger and such relativistic electron scattering processes become more significant. As sophisticated theoretical solutions evolve, more accurate experimental data are required to test these theoretical models for the electron scattering from heavy inert gases and vice-versa. We have now conducted a similar experiment to that performed in Xe by Khakoo *et al* (1996a, b), in Kr, i.e. a target like Xe in structure, but with lower Z values, in an effort to observe reduced, but nevertheless significant, spin-orbit effects in the scattering channels.

Earlier measurements concerning absolute DCSs for Kr have been reported by Trajmar *et al* (1981), Filipovic (1988) and Danjo (1988, 1989). Other collision parameters for inelastic electron scattering from rare gases are available from experimental studies of, e.g., polarized electron scattering asymmetries (Dümmler *et al* 1995), Stokes parameters of the light emitted following the impact excitation by polarized or unpolarized electrons, (Furst *et al* 1993, Norén and McConkey 1996, Norén *et al* 1996, Yu *et al* 1997a, b, Zeman *et al* 1998a, b), coherence and correlation parameters (Becker *et al* 1992), etc. Ratios of DCSs have been introduced as useful collision parameters by Khakoo *et al* (1992, 1994) and very recently by Guo *et al* (1999). A summary of available electron-impact excitation DCSs of the rare gases (theory and experiment) is given by Khakoo *et al* (1994).

Conventional measurements of absolute inelastic DCSs rely on normalization of inelastic electron scattering intensities to elastic scattering intensities and require the availability of accurate elastic differential cross section calibrations (see for example, Khakoo *et al* 1996a, b).

This process makes it difficult to measure inelastic differential cross sections with errors less than 15–30%. Experiments measuring coherence or correlation parameters while providing different details of the scattering process are usually very difficult and suffer from poorer statistics than conventionally measured DCSs. Consequently the availability of such coherence or correlation data is limited.

The use of DCS ratios as an alternative set of parameters has been recently highlighted for Kr (Guo *et al* 1999). These DCS ratios can be determined with high accuracy for heavy rare gases and have been investigated both experimentally (Register *et al* 1980, Khakoo *et al* 1992, 1994 and 1996a) and theoretically (Bartschat and Madison 1992, Fontes 1998). Such ratios can be measured more readily than absolute differential cross sections or scattering parameters, to provide more reliable data for testing theoretical models.

DCS ratios for the first four excitation levels of Kr are defined as follows:

$$r = \frac{\sigma(5s[3/2]_2)}{\sigma(5s'[1/2]_0)}, \quad r' = \frac{\sigma(5s[3/2]_1)}{\sigma(5s'[1/2]_1)}, \quad r'' = \frac{\sigma(5s[3/2]_2)}{\sigma(5s[3/2]_1)}. \quad (1)$$

The $4p^55s$ levels in Kr can be expressed in the simplified intermediate-coupling scheme (Cowan 1981) with only one configuration as:

$$\begin{aligned} |5s[3/2]_2\rangle &= |5^3P_2\rangle; \\ |5s[3/2]_1\rangle &= \alpha |5^3P_1\rangle - \beta |5^1P_1\rangle; \\ |5s'[1/2]_0\rangle &= |5^3P_0\rangle; \\ |5s'[1/2]_1\rangle &= \alpha |5^1P_1\rangle + \beta |5^3P_1\rangle. \end{aligned} \quad (2)$$

Here α and β are the intermediate-coupling (unitary) mixing coefficients. The single configuration values of (α, β) based on the Cowan code (12-configuration model) used by the UFOMBT and those generated by the RM code are $(-0.673, 0.735)$ and $(-0.739, 0.674)$, respectively. We note the apparent reversal in the magnitude of α and β between the UFOMBT and the RM models. The effect of this difference in the structure calculation will be seen most prominently in the r' results discussed in section 4 below. Mixing coefficients associated with additional configurations were at least one order of magnitude smaller than α and β .

From equations (2), we see that r considers excitations to optically forbidden levels, excitable only via spin-exchange, in the above coupling scheme. In the limiting case of degenerate fine-structure levels (Khakoo *et al* 1992), where spin-orbit interactions are absent, r attains its LS coupling limit of 5, i.e. the statistical weight ratio of the respective levels, with $J = 2$ and $J = 0$. On the other hand, r' considers excitations to the optically allowed $J = 1$ levels. However, these levels have mixed triplet-singlet character. In the optical limit (high incident electron energy and small scattering angle), application of dipole selection rules reveals, within this single-configuration coupling scheme, a limit for r' :

$$\lim_{E_0 \rightarrow \infty} r' = \beta^2 / \alpha^2. \quad (3)$$

Deviation from the optical limit could indicate the importance of the triplet part of the $J = 1$ levels or additional singlet levels which are needed to describe these mixed levels. The third parameter r'' provides additional information on the coupling scheme needed to describe the metastable, optically forbidden levels relative to the optically allowed levels, and consequently completes the framework of these ratios (Guo *et al* 1999).

In this paper, which is the first in a back-to-back series of two (from here on referred to as part I), we present recently obtained measurements of absolute DCSs and DCS ratios for electron-impact excitation from the ground $[4p^6(^1S_0)]$ level of Kr to the $4p^55s$ ($5s[3/2]_2$, $5s[3/2]_1$, $5s'[1/2]_0$ and $5s'[1/2]_1$) levels. Part II concerns excitation of the next energetically higher excited Kr levels which constitute the $4p^55p$, $4p^54d$ and $4p^56s$ configurations. The

experimental results are compared with our most recent calculations based on the RM and UFOMBT models. These models will be described in section 2, followed by experimental details in section 3. Both experimental and theoretical data and the comparison between them will be presented in section 4. The summary and conclusions will be presented in section 5.

2. Theoretical models

2.1. R-matrix

The R-matrix calculations reported here were performed along the lines described in detail by Zeman and Bartschat (1997) for electron-impact excitation of Ne, and the most important aspects were summarized again by Zeman *et al* (1998b). Very briefly, the N -electron target states were represented as multi-configuration expansions through diagonalization of the target Hamiltonian. The configurations themselves were constructed from a bound orbital basis whose radial components were generated with the atomic structure package CIV3 of Hibbert (1975). After the non-relativistic orbitals had been obtained, the one-electron relativistic mass correction, Darwin and spin-orbit terms were added in first-order perturbation theory in the diagonalization of the target Hamiltonian. The largest calculation performed included the 31 target states with the configurations $4p^6$, $4p^55s$, $4p^55p$, $4p^54d$ and $4p^56s$. Smaller calculations were restricted to the first 5 and 15 states. Due to the complexity of these calculations, we used the same set of one-electron orbitals to describe all 31 states—although it would, in principle, be possible to optimize the orbitals in such a way that the states involved in a given transition are heavily favoured, the computational demands of such an approach are prohibitive. As a result, however, the quality of the target description may suffer. The consequences of using one-electron orbitals generally become most visible when an accurate target description is more important than channel coupling. Some examples of this effect will be discussed below.

The collision calculations were performed in the standard R-matrix formulation of the close-coupling approach. It is based upon the partitioning of configuration space into two regions, $r \leq a$ and $r \geq a$, where the radius a is defined in such a way that exchange effects can be neglected in the outer region. The radial wavefunction of the projectile electron in the inner region is then expanded in terms of a basis set and used to form the channel functions. The advantage of this method lies in the fact that the solution of a coupled set of integro-differential equations for each total collision energy, E , that is characteristic of a standard close-coupling approach, is replaced by a single matrix diagonalization for each partial-wave symmetry of the $(N + 1)$ -electron Hamiltonian. The solution is then matched to that of a much simpler system of coupled ordinary differential equations in the external region that yields the transition matrix elements of interest.

2.2. The unitarized first-order many-body theory

The UFOMBT results were calculated in a manner very similar to that described in Khakoo *et al* (1996a) and therefore only a very brief description is provided. A 12-configuration basis set was used in carrying out Hartree-Fock atomic structure calculations with the CATS code (Abdallah *et al* 1988). The ACE code (Clark *et al* 1988) was then used to determine the UFOMBT excitation cross sections. The importance of the $4p^54d$ configuration for the present Kr results, as well as the analogous effect on excitation in Xe, has been reported in an earlier article (Fontes 1998).

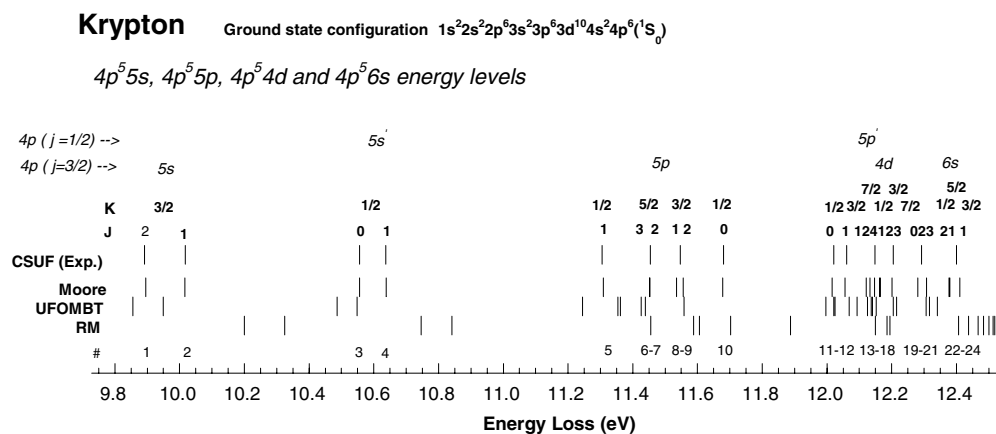


Figure 1. Graphic illustration of the pertinent Kr energy levels and their designations. CSUF (Exp.): the present experimental result, with the energy scale normalized to Moore's spectroscopic data at the second ($5s[3/2]_1$) and fourth ($5s'[1/2]_1$) levels; Moore: spectroscopic result (Moore 1952); UFOMBT: energy scale given by the present UFOMBT calculation; RM: energy scale given by the present RM calculation. The intermediate coupling ($J-K$) notation is used (see e.g. Cowan *et al* 1981). The designation follows that of Moore (1952).

2.3. Comparison of structure results

Theoretical energy levels for Kr, as obtained within the RM code and by the Cowan code (used by the UFOMBT) are shown in figure 1. We note that the Cowan code yields results significantly closer to Moore's spectroscopic energy levels (Moore 1952) than those obtained within the 'averaged-orbital' R-matrix method described above. The designations of the Kr features (using JL -coupling, Cowan, 1981) as labelled in the Kr spectrum in figure 2 are given in table 1. Table 2 gives the dominant expansion coefficients (> 0.1) for the various Kr levels in terms of the intermediate-coupling scheme, as obtained by the Cowan code.

3. Experimental

3.1. Experimental apparatus

We used a state-of-the-art electron energy-loss spectrometer with double hemispherical energy selectors in both the gun and the analyser sections, similar to that used by Register *et al* (1980). The spectrometer is housed in a clean vacuum chamber (base pressure of the vacuum chamber is 1×10^{-7} Torr) which is pumped with a 12" diffusion pump. Both the gun and the analyser sections were baked to about 120°C during the experiment to maintain stable conditions necessary for taking electron energy-loss spectra over long periods of time. To reduce effects from the earth's magnetic field, the vacuum chamber is shielded with double mu-metal layers. The double layer shield is further demagnetized and the magnetic field in the chamber is reduced to 1–2 mG. An important feature of this spectrometer is the absence of 'wings' in the instrumental profile, often seen in spectrometers with single hemispherical analysers. This feature enabled us to resolve the weak metastable energy-loss features from the stronger allowed transitions in Kr. The spectrometer operated at an energy resolution of 30–40 meV with electron currents ranging from 3–20 nA. It could observe scattered electrons at scattering angles (θ) up to 135° . A typical electron energy-loss spectrum measured at 95°

Table 1. Designations and grouping of levels comprising features observed in the energy-loss spectra of Kr (see figures 1 and 2). The twenty-four levels are grouped into twelve features that can be resolved with our spectrometer. The table provides a comparison of groupings based on the energy level values from the UFOMBT (Cowan code), RM, and that of Moore (1952) (see also NSRDS-NBS 1972) and NSRDS-NBS (NBS 1972).

Features	1	2	3	4	5	6	7	8
Levels	1	2	3	4	5	6+7	8+9	10
Moore	5s[3/2] ₂	5s[3/2] ₁	5s'[1/2] ₀	5s'[1/2] ₁	5p[1/2] ₁	5p[5/2] ₃ + 5p[5/2] ₂	5p[3/2] ₁ + 5p[3/2] ₂	5p[1/2] ₀
UFOMBT	5s[3/2] ₂	5s[3/2] ₁	5s'[1/2] ₀	5s'[1/2] ₁	5p[1/2] ₁	5p[5/2] ₃ + 5p[5/2] ₂	5p[3/2] ₁ + 5p[3/2] ₂	5p[1/2] ₀
RM	5s[3/2] ₂	5s[3/2] ₁	5s'[1/2] ₀	5s'[1/2] ₁	5p[1/2] ₁	5p[5/2] ₃ + 5p[5/2] ₂	5p[3/2] ₁ + 5p[3/2] ₂	5p[1/2] ₀
Features	9		10			11	12	
Levels	11+12		13–18			19–21	22–24	
Moore	4d[1/2] ₀ + 4d[1/2] ₁		5p'[3/2] ₁ + 4d[3/2] ₂ + 4d[7/2] ₄ +5p'[1/2] ₁ + 5p'[3/2] ₂ + 4d[7/2] ₃			5p'[1/2] ₀ + 4d[5/2] ₂ +4d[5/2] ₃	6s[3/2] ₂ + 4d[3/2] ₁ + 6s[3/2] ₁	
UFOMBT	5p'[3/2] ₁ + 5p'[1/2] ₁		5p'[3/2] ₂ + 4d[1/2] ₀ + 4d[1/2] ₁ +4d[7/2] ₄ + 4d[3/2] ₂ + 5p'[1/2] ₀			4d[7/2] ₃ + 4d[5/2] ₂ +4d[5/2] ₃	6s[3/2] ₂ + 4d[3/2] ₁ + 6s[3/2] ₁	
RM	5p'[3/2] ₁		5p'[3/2] ₂ + 5p'[1/2] ₁			5p'[1/2] ₀	6s[3/2] ₂ + 6s[3/2] ₁ + 4d[1/2] ₀ +4d[1/2] ₁ + 4d[7/2] ₄ + 4d[7/2] ₃ +4d[3/2] ₂ + 4d[3/2] ₁ +4d[5/2] ₂ + 4d[5/2] ₃	

Table 2. The most significant intermediate-coupling coefficients (> 0.1) for the pertinent levels of Kr derived from the lowest four configurations ($4p^55s$, $4p^55p$, $4p^54d$ and $4p^56s$) obtained from the Cowan code used in the UFOMBT. The energy values are taken from Moore (1952).

Level	$J-L$ coupling	Intermediate coupling (dominant levels)	Energy (eV), Cowan	Energy (eV), Moore
1	$4p^6$	$0.9983(4p^6 \ ^1S_0)$	0	0
2	$4p^55s [3/2]_2$	$0.9983 (4p^55s \ ^3P_2)$	9.876	9.915
3	$4p^55s [3/2]_1$	$0.6731 (4p^55s \ ^3P_1) + 0.7381 (4p^55s \ ^1P_1)$	9.969	10.033
4	$4p^55s' [1/2]_0$	$0.9961 (4p^55s \ ^3P_0)$	10.495	10.563
5	$4p^55s' [1/2]_1$	$0.7354 (4p^55s \ ^3P_1) - 0.6738 (4p^55s \ ^1P_1)$	10.556	10.644
6	$4p^55p [1/2]_1$	$-0.3751 (4p^55p \ ^3P_1) + 0.8989 (4p^55p \ ^3S_1) + 0.2169 (4p^55p \ ^1P_1)$	11.240	11.304
7	$4p^55p [5/2]_3$	$0.9979 (4p^55p \ ^3D_3)$	11.349	11.443
8	$4p^55p [5/2]_2$	$0.7068 (4p^55p \ ^3D_2) - 0.1666 (4p^55p \ ^3P_2) + 0.6873 (4p^55p \ ^1D_2)$	11.355	11.445
9	$4p^55p [3/2]_1$	$-0.4666 (4p^55p \ ^3D_1) + 0.4967 (4p^55p \ ^3P_1) + 0.7305 (4p^55p \ ^1P_1)$	11.419	11.526
10	$4p^55p [3/2]_2$	$-0.2163 (4p^55p \ ^3D_2) + 0.8742 (4p^55p \ ^3P_2) + 0.4343 (4p^55p \ ^1D_2)$	11.431	11.546
11	$4p^55p [1/2]_0$	$-0.6828 (4p^55p \ ^3P_0) + 0.7238 (4p^55p \ ^1S_0)$	11.548	11.666
12	$4p^54d [1/2]_0$	$0.9927 (4p^54d \ ^3P_0)$	12.049	11.998
13	$4p^54d [1/2]_1$	$0.9346 (4p^54d \ ^3P_1) - 0.1184 (4p^54d \ ^1P_1) - 0.3077 (4p^54d \ ^3D_1)$	12.074	12.037
14	$4p^55p' [3/2]_1$	$0.8653 (4p^55p \ ^3D_1) + 0.1147 (4p^55p \ ^3P_1) + 0.4793 (4p^55p \ ^1P_1)$	11.979	12.101
15	$4p^54d [3/2]_2$	$-0.4667 (4p^54d \ ^3D_2) + 0.7823 (4p^54d \ ^3P_2) + 0.3740 (4p^54d \ ^1D_2) + 0.1589 (4p^56s \ ^3P_2)$	12.116	12.112
16	$4p^54d [7/2]_4$	$0.9992 (4p^54d \ ^3F_4)$	12.105	12.126
17	$4p^55p' [1/2]_1$	$0.1802 (4p^55p \ ^3D_1) + 0.7733 (4p^55p \ ^3P_1) + 0.4195 (4p^55p \ ^3S_1) - 0.4342 (4p^55p \ ^1P_1)$	12.004	12.141
18	$4p^55p' [3/2]_2$	$0.6730 (4p^55p \ ^3D_2) + 0.4555 (4p^55p \ ^3P_2) - 0.5819 (4p^55p \ ^1D_2)$	12.007	12.144
19	$4p^54d [7/2]_3$	$0.7486 (4p^54d \ ^3F_3) - 0.1751 (4p^54d \ ^3D_3) + 0.6391 (4p^54d \ ^1F_3)$	12.131	12.179
20	$4p^55p' [1/2]_0$	$0.7297 (4p^55p \ ^3P_0) + 0.6702 (4p^55p \ ^1S_0) - 0.1304 (4p^56p \ ^1S_0)$	12.120	12.257
21	$4p^54d [5/2]_2$	$-0.5376 (4p^54d \ ^3F_2) + 0.5301 (4p^54d \ ^3D_2) + 0.6550 (4p^54d \ ^1D_2)$	12.184	12.258
22	$4p^54d [5/2]_3$	$-0.2310 (4p^54d \ ^3F_3) + 0.8343 (4p^54d \ ^3D_3) + 0.4994 (4p^54d \ ^1F_3)$	12.194	12.284
23	$4p^56s [3/2]_2$	$0.1046 (4p^54d \ ^3D_2) + 0.9851 (4p^56s \ ^3P_2)$	12.293	12.352
24	$4p^54d [3/2]_1$	$-0.6645 (4p^54d \ ^3D_1) + 0.7014 (4p^54d \ ^1P_1) - 0.1427 (4p^55d \ ^1P_1)$ $-0.1373 (4p^56s \ ^1P_1) - 0.1039 (4p^56s \ ^3P_1) - 0.1117 (4p^54d \ ^3P_1)$	12.283	12.354
25	$4p^56s [3/2]_1$	$0.1386 (4p^54d \ ^1P_1) + 0.5858 (4p^56s \ ^3P_1) + 0.7866 (4p^56s \ ^1P_1)$	12.317	12.385

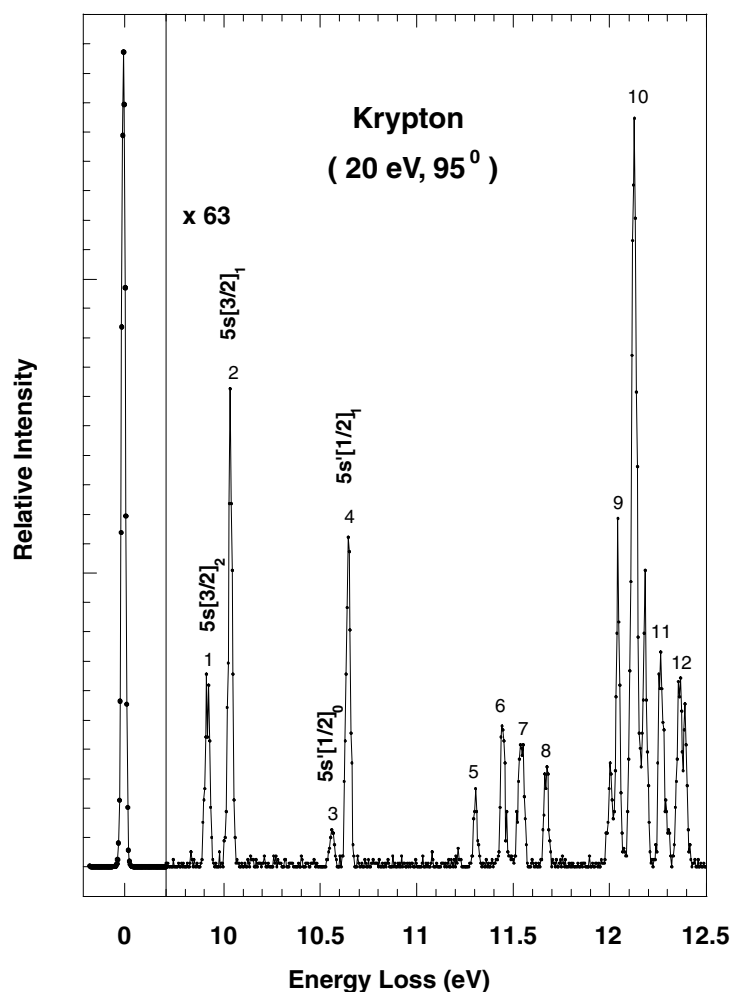


Figure 2. Energy-loss spectrum of Kr. The resolution of the spectrometer is 29 meV (FWHM). Features are labelled as in table 1.

with 20 eV incident electrons is shown in figure 2. At the upper limit of the energy resolution (30 meV, 3 nA), it was not necessary to unfold the spectra for the first four transitions in Kr.

The apparatus is computer-controlled to enable efficient data acquisition. The computer processes the experimental results from the energy-loss scan and controls the scattering angle positioning. It monitors the pressure behind the gas line and modulates the gas beam via a thin molybdenum beam flag. Analysis of the measured spectra is done off-line. A sophisticated multi-Gaussian unfolding program which has been well tested (Khakoo *et al* 1994, 1996a, b) is used to unfold the spectra. Here, the instrumental profile for the unfolding was obtained by a multi-Gaussian fit (typically two to three Gaussians) to an isolated energy-loss feature (e.g. feature 2, or the elastic peak at 0 eV energy loss; see figure 2). The energy levels of Kr from Moore's spectroscopy tables (Moore 1952) are used in the unfolding program. Typical reduced chi-squared (χ^2) values of the fits to the spectra were in the range of 1–3.

3.2. Spectrometer calibration

The incident electron beam kinetic energy (E_0) was calibrated to within ± 0.05 eV by measuring the 2^2S resonance of He at 19.366 eV (Brunt *et al* 1977). The angular calibration of the spectrometer was performed using characteristic minima in elastic scattering from Xe and Ar (Register *et al* 1980, Srivastava *et al* 1981, Danjo 1988) and is estimated to be accurate to $\pm 1^\circ$.

The detection efficiency (or transmission function) of the analyser for scattered electrons is, to first order, proportional to the residual energy ($E_R = E_0 - \Delta E$, where ΔE is the electron energy loss) of the electrons. This transmission function $\xi(E_R)$ needs to be measured to extract DCSs from our energy-loss spectra.

For this calibration, the conventional method using the He ionization continuum (Pichou *et al* 1978), as extended by Nickel *et al* (1989) was employed. At an incident electron energy of 30.58 eV and $\theta = 90^\circ$, the scattered electron signal was measured for the energy-loss range of 20–29.5 eV which covers both the $n = 2, 3$ and 4 manifold excitations and the ionization continuum. The He ionization continuum corresponds to an E_R range of 6 eV to 1 eV. This covers the residual energy range for the Kr measurements for incident energies of 15.0, 13.5 and 12.0 eV and yields a response function over the 6 eV to 1 eV E_R range. Figure 3 shows the

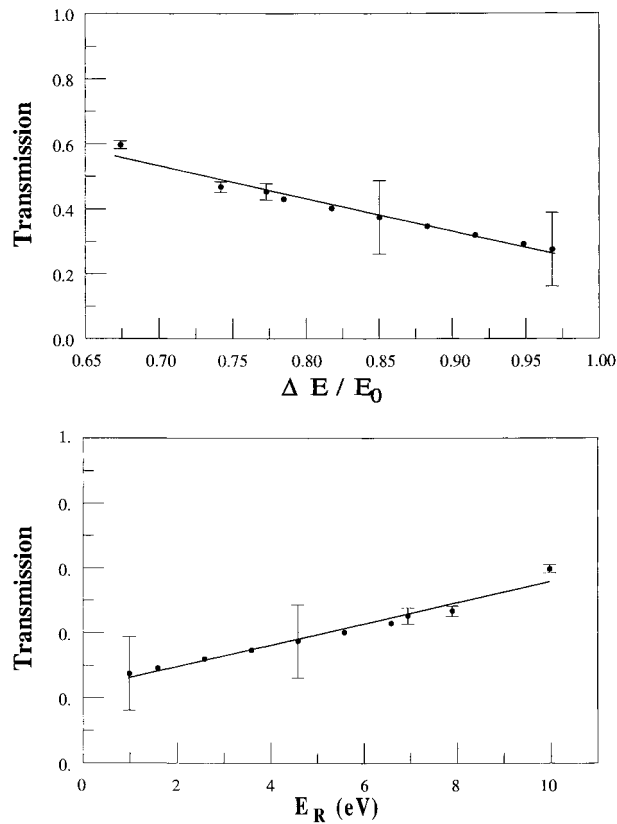


Figure 3. Measurement of the relative analyser detection efficiency $\xi(E_R)$ (transmission) using the He ionization method. The efficiency for transmission was set to unity for elastic scattering. ΔE is the energy loss and E_0 is the incident electron energy in the same units. E_R is the residual electron energy. See section 3.2 for details.

spectrometer function $\xi(E_R)$ deduced from the He measurements. The relative transmission function for the 6 eV to 10 eV E_R region was determined by normalizing the scattering intensity for the measured $n = 2, 3$ and 4 level excitations to He DCSs obtained by Bray (1998). We found that $\xi(E_R)$ is a linear function in E_R with a positive slope.

3.3. Determination of DCS ratios and absolute DCSs

The inelastic spectra were unfolded using our spectrum-unfolding code and the line intensities from the unfolding procedure were corrected for the variation of $\xi(E_R)$. These corrected line intensities were used to determine the DCS ratios given in equations (1). Typical errors involved in $\xi(E_R)$ across the spectrum (which depend on the variation of this function which is essentially linear) incurred an error of 1–5% in these ratios, being largest at the lowest incident electron energy. To normalize the spectral intensities to the absolute scale, we employed the elastic DCSs of Danjo (1988). The elastic peak and the inelastic features were scanned together and their intensity ratios were determined. The background associated with elastic scattering was a more significant proportion of the signal than the inelastic background of its corresponding measured signal. These background contributions were accurately determined by interrupting the gas beam at the collision region (using a thin molybdenum chopper). At $E_0 = 20$ eV, the elastic scattering background was about 2–3% of the signal, whereas at $E_0 = 12.5$ eV it had increased to about 25%.

In this method, the major contribution to the uncertainty in the absolute inelastic cross sections is from the elastic DCSs, which is typically 20% (Danjo 1988). This was incorporated into inelastic/elastic ratio determinations. For the two optically forbidden levels ($5s[3/2]_2$ and $5s'[1/2]_0$) the uncertainty in the absolute differential cross sections is largely reduced since the ratios of the $5s[3/2]_2$ and $5s'[1/2]_0$ levels relative to the allowed $5s[3/2]_1$ and $5s'[1/2]_1$ (respectively) can be measured accurately. For example, the cross sections of the optically forbidden level $5s[3/2]_2$ could be determined by $DCS(5s[3/2]_2) = r'' DCS(5s[3/2]_1)$, where the ratio r'' can be accurately measured with our high resolution spectrometer with a 1–2% uncertainty, since both features lie next to each other and thus have almost the same $\xi(E_R)$.

From figure 2 we observe that the two optically allowed levels ($5s[3/2]_1$ and $5s'[1/2]_1$) have much higher intensities than those of the optically forbidden levels ($5s[3/2]_2$ and $5s'[1/2]_0$). At small scattering angles the relative intensities of the two optically forbidden levels compared to the optically allowed levels are even weaker than those shown in figure 2. Therefore the conventional inelastic–elastic peak ratio method was first used to determine the absolute differential cross sections for the two optically allowed levels, then we determined the absolute DCSs of the two optically forbidden levels based on our differential cross section ratios.

3.4. Errors encountered in the experiments

A summary of encountered errors is given in table 3. In the determination of line intensities, errors encountered in these measurements consist of the statistical error plus errors induced in

Table 3. Summary of observed errors (1 standard deviation) in the present experiment.

E_0 (eV)	20.0	15.0	13.5	12.0
Fitting/Statistics	3.8%	4.9%	5.6%	5.8%
Transmission	2.5%	3.4%	3.8%	4.4%
Elastic DCS (Danjo, 1988)	20%	20%	20%	20%

fitting the spectra. The uncertainty in the determination of $\xi(E_R)$ across the spectrum affects the intensity ratios, whereas uncertainties in the elastic to inelastic calibrations in the elastic DCS values of Danjo (1988) contribute to the determination of absolute DCS for the inelastic features. Only the statistical errors in the determination of $\xi(E_R)$ are quoted and systematic errors in this method were not estimated. During the period of these measurements, data were repeated and the intensity ratios were checked for reproducibility and weighted-averaged to reduce error bars.

4. Results and discussion

Measurements and RM and UFOMBT calculations were made at electron incident energies below and above the ionization threshold of Kr (13.996 eV; Kuhn 1962) for scattering angles ranging from 10° – 135° . For the incident energies above the ionization threshold, $E_0 = 15.0$ eV and 20.0 eV, we compare the present results with the existing experimental data (DCSs: Trajmar *et al* 1981; DCS ratios: Khakoo *et al* 1994). Thus we can provide a comprehensive test of the RM and the UFOMBT calculations. For the energies below the ionization threshold, $E_0 = 12.0$ eV and 13.5 eV, we attempted to stay in regions free of resonance effects (see e.g. Phillips 1982). The experimental results are tabulated in tables 4–7 for the energies of 20.0 eV, 15.0 eV, 13.5 eV and 12.0 eV, respectively, and are compared with the theoretical models and other experimental results in figures 4(a)–(d) for the DCS ratios and in figures 5(a)–(d) for the DCS. As mentioned previously in Guo *et al* 1999, the DCS ratios are expected to provide a more sensitive test of different theoretical methods and are discussed first.

4.1. DCS ratios (r , r' and r'')

The measured ratios at incident electron energies above the ionization threshold are shown in figures 4(a) and (b) together with theoretical results from R-matrix, UFOMBT and RDWA calculations. We have also included the DCS ratios measured by Khakoo *et al* (1994). We did not include the ratio measurements of Filipovic *et al* (1988) because these were found to be too scattered (see ratio comparisons in Khakoo *et al* 1994). We also do not include in our comparison the DCS ratios from the measurements of Trajmar *et al* (1981), to avoid congestion of the graphs. In general, the DCS ratios of Trajmar *et al* (1981) were found to be in good agreement with the present values, but had considerably larger error bars throughout.

4.1.1. $E_0 = 20.0$ eV In figure 4(a), at $E_0 = 20.0$ eV, the ratio r has a value of around 5 and shows good agreement with the RM, the UFOMBT and the RDWA results at small angles. At this energy we observe that the R-matrix results are rather insensitive to the number of states included in the calculation (note that only the 31-state RM is shown in these plots to avoid congestion). The ‘dip’ structure around 60° (r dropping below the value of 4) is observed clearly in the present and previous experiments (Khakoo *et al* 1994). These two are in very good agreement (within error bars), except that the earlier data (Khakoo *et al* 1994) are slightly lower. This dip is not reproduced by any of the models. A similar ‘dip’ structure around 60° is also observed by Trajmar *et al* (1981). This discrepancy between the experiments and the theories is not as obvious in the cross sections (see figure 5(a)) as in the ratios.

For the ratio r' , the present data are in excellent agreement with those of Khakoo *et al* (1994). The results from the UFOMBT are also in excellent agreement with the experimental data. One would also expect the UFOMBT to give excellent agreement since it does a good job of modelling states strongly coupled to the ground state. However, the R-matrix model shows significantly lower values but maintains qualitative agreement with the experiments. We note

Table 4. DCS Ratios and DCSs for the electron-impact excitation of Kr for $E_{in} = 20.0$ eV. The digits in brackets refer to the uncertainty (least significant digits; 1 standard deviation) in the DCSs. See table 3 for a summary of error sources.

θ (deg)	r	r'	r''	$5s[3/2]_2$ (10^{-18} cm 2 sr $^{-1}$)	$5s[3/2]_1$ (10^{-18} cm 2 sr $^{-1}$)	$5s'[3/2]_0$ (10^{-18} cm 2 sr $^{-1}$)	$5s'[1/2]_1$ (10^{-18} cm 2 sr $^{-1}$)
10	4.80 (1.00)	1.51 (0.02)	0.09 (0.01)	2.03 (0.50)	21.51 (4.34)	0.42 (0.14)	14.19 (2.87)
15	5.11 (0.51)	1.50 (0.02)	0.13 (0.01)	1.73 (0.36)	13.48 (2.72)	0.34 (0.08)	8.54 (1.73)
20	5.14 (0.25)	1.46 (0.02)	0.19 (0.01)	1.44 (0.31)	7.68 (1.56)	0.28 (0.06)	5.06 (1.03)
25	4.74 (0.33)	1.36 (0.02)	0.26 (0.01)	1.48 (0.30)	5.71 (1.15)	0.31 (0.07)	4.16 (0.84)
30	5.00 (0.28)	1.39 (0.02)	0.28 (0.01)	1.40 (0.28)	5.10 (1.03)	0.28 (0.06)	3.68 (0.74)
35	5.35 (0.60)	1.27 (0.04)	0.27 (0.01)	1.25 (0.25)	4.58 (0.92)	0.23 (0.05)	3.60 (0.73)
40	4.98 (0.23)	1.29 (0.07)	0.25 (0.01)	0.98 (0.21)	3.97 (0.80)	0.20 (0.04)	3.08 (0.62)
45	4.88 (0.69)	1.22 (0.03)	0.22 (0.01)	0.85 (0.18)	3.94 (0.80)	0.18 (0.04)	3.30 (0.67)
50	4.41 (0.50)	1.20 (0.02)	0.17 (0.01)	0.59 (0.12)	3.37 (0.68)	0.13 (0.03)	2.78 (0.56)
55	3.93 (0.39)	1.21 (0.02)	0.17 (0.01)	0.45 (0.09)	2.72 (0.55)	0.12 (0.03)	2.23 (0.45)
60	4.03 (0.37)	1.16 (0.02)	0.19 (0.01)	0.47 (0.10)	2.51 (0.51)	0.12 (0.03)	2.16 (0.44)
65	3.88 (0.69)	1.19 (0.05)	0.20 (0.01)	0.48 (0.14)	2.34 (0.69)	0.12 (0.04)	1.97 (0.59)
70	4.22 (0.42)	1.19 (0.03)	0.25 (0.01)	0.43 (0.09)	1.72 (0.35)	0.10 (0.02)	1.45 (0.29)
75	5.01 (0.50)	1.15 (0.03)	0.32 (0.01)	0.45 (0.09)	1.42 (0.29)	0.09 (0.02)	1.24 (0.25)
80	4.12 (0.53)	1.19 (0.05)	0.38 (0.01)	0.35 (0.07)	0.93 (0.19)	0.09 (0.02)	0.80 (0.16)
85	4.97 (0.67)	1.11 (0.03)	0.43 (0.02)	0.36 (0.08)	0.85 (0.17)	0.07 (0.02)	0.76 (0.16)
90	4.74 (0.34)	1.15 (0.02)	0.42 (0.04)	0.30 (0.07)	0.71 (0.15)	0.06 (0.02)	0.63 (0.13)
95	4.44 (0.31)	1.13 (0.02)	0.40 (0.02)	0.25 (0.05)	0.62 (0.13)	0.06 (0.01)	0.55 (0.11)
100	5.17 (0.45)	1.04 (0.03)	0.49 (0.02)	0.27 (0.06)	0.55 (0.11)	0.05 (0.01)	0.50 (0.10)
105	5.13 (0.64)	1.11 (0.04)	0.48 (0.02)	0.37 (0.08)	0.78 (0.16)	0.07 (0.02)	0.70 (0.14)
110	4.26 (0.60)	1.03 (0.04)	0.49 (0.09)	0.39 (0.11)	0.80 (0.17)	0.09 (0.03)	0.77 (0.16)
115	4.69 (0.59)	1.08 (0.05)	0.54 (0.06)	0.44 (0.10)	0.82 (0.17)	0.09 (0.03)	0.73 (0.15)
120	4.37 (0.26)	1.06 (0.06)	0.58 (0.02)	0.47 (0.10)	0.82 (0.17)	0.11 (0.02)	0.79 (0.16)
125	3.90 (0.35)	0.98 (0.04)	0.58 (0.02)	0.53 (0.11)	0.92 (0.19)	0.14 (0.03)	0.85 (0.17)
130	4.23 (0.63)	1.04 (0.06)	0.64 (0.04)				

Table 5. As table 4, but for $E_{in} = 15.0$ eV.

θ (deg)	r	r'	r''	$5s[3/2]_2$ (10^{-18} cm 2 sr $^{-1}$)	$5s[3/2]_1$ (10^{-18} cm 2 sr $^{-1}$)	$5s'[3/2]_0$ (10^{-18} cm 2 sr $^{-1}$)	$5s'[1/2]_1$ (10^{-18} cm 2 sr $^{-1}$)
10	4.10 (1.47)	1.99 (0.11)	0.04 (0.00)	0.42 (0.09)	11.76 (2.39)	0.10 (0.04)	5.97 (1.22)
15	3.07 (0.69)	1.89 (0.02)	0.06 (0.01)	0.43 (0.11)	7.15 (1.45)	0.14 (0.05)	4.12 (0.84)
20	4.30 (0.79)	1.76 (0.04)	0.13 (0.01)	0.44 (0.10)	3.45 (0.70)	0.10 (0.03)	2.09 (0.43)
25	3.45 (0.89)	1.64 (0.05)	0.17 (0.01)	0.57 (0.12)	3.39 (0.69)	0.17 (0.06)	2.28 (0.47)
30	5.00 (0.68)	1.49 (0.04)	0.30 (0.03)	0.78 (0.18)	2.62 (0.54)	0.16 (0.04)	1.81 (0.37)
35	5.59 (0.40)	1.32 (0.02)	0.40 (0.05)	0.98 (0.23)	2.47 (0.50)	0.18 (0.04)	1.91 (0.39)
40	6.16 (0.78)	1.41 (0.03)	0.44 (0.02)	1.00 (0.21)	2.29 (0.47)	0.16 (0.04)	1.70 (0.35)
45	5.03 (0.34)	1.36 (0.03)	0.39 (0.10)	0.95 (0.31)	2.47 (0.50)	0.19 (0.06)	1.83 (0.37)
50	5.53 (0.34)	1.33 (0.03)	0.46 (0.01)	1.17 (0.24)	2.56 (0.52)	0.21 (0.05)	1.81 (0.37)
55	6.93 (0.84)	1.36 (0.02)	0.46 (0.02)	1.62 (0.35)	3.55 (0.76)	0.23 (0.06)	2.54 (0.55)
60	7.74 (0.87)	1.35 (0.05)	0.50 (0.02)	1.82 (0.38)	3.69 (0.75)	0.24 (0.06)	2.91 (0.59)
65	6.03 (0.54)	1.35 (0.04)	0.58 (0.02)	1.61 (0.33)	2.76 (0.56)	0.27 (0.06)	1.79 (0.37)
70	6.58 (0.42)	1.37 (0.03)	0.62 (0.03)	2.39 (0.50)	3.83 (0.78)	0.36 (0.08)	2.77 (0.56)
75	5.91 (0.87)	1.33 (0.06)	0.65 (0.03)	1.51 (0.32)	2.31 (0.47)	0.26 (0.07)	1.54 (0.32)
80	7.63 (0.82)	1.24 (0.04)	0.72 (0.02)	1.57 (0.32)	2.17 (0.44)	0.21 (0.05)	1.75 (0.36)
85	5.82 (0.68)	1.34 (0.08)	0.73 (0.04)	1.09 (0.24)	1.47 (0.31)	0.17 (0.04)	1.10 (0.24)
90	6.32 (0.77)	1.24 (0.04)	0.56 (0.02)	0.90 (0.19)	1.59 (0.33)	0.14 (0.03)	1.26 (0.26)
95	4.43 (0.80)	1.22 (0.11)	0.64 (0.06)	0.90 (0.21)	1.38 (0.30)	0.18 (0.05)	1.13 (0.25)
100	4.79 (0.82)	1.22 (0.05)	0.52 (0.05)	0.65 (0.15)	1.24 (0.26)	0.14 (0.04)	1.08 (0.23)
105	3.68 (0.68)	1.07 (0.09)	0.49 (0.04)	0.74 (0.19)	1.60 (0.35)	0.13 (0.06)	1.35 (0.30)
110	5.00 (0.41)	1.13 (0.04)	0.50 (0.02)	1.05 (0.22)	2.13 (0.43)	0.21 (0.05)	1.90 (0.39)
115	5.88 (0.51)	1.18 (0.04)	0.50 (0.02)	1.25 (0.26)	2.52 (0.51)	0.21 (0.05)	2.21 (0.45)
120	5.27 (0.39)	1.19 (0.03)	0.56 (0.02)	1.49 (0.31)	2.64 (0.54)	0.28 (0.06)	2.25 (0.46)
125	5.11 (0.35)	1.14 (0.04)	0.55 (0.02)	1.50 (0.31)	2.70 (0.55)	0.29 (0.06)	2.44 (0.50)
130	5.68 (0.45)	1.19 (0.03)	0.54 (0.02)	1.16 (0.24)	2.14 (0.44)	0.21 (0.05)	1.87 (0.38)

Table 6. As table 4, but for $E_{\text{in}} = 13.5$ eV.

θ (deg)	r	r'	r''	$5s[3/2]_2$ ($10^{-18} \text{ cm}^2 \text{ sr}^{-1}$)	$5s[3/2]_1$ ($10^{-18} \text{ cm}^2 \text{ sr}^{-1}$)	$5s'[3/2]_0$ ($10^{-18} \text{ cm}^2 \text{ sr}^{-1}$)	$5s'[1/2]_1$ ($10^{-18} \text{ cm}^2 \text{ sr}^{-1}$)
10	6.39 (1.36)	2.58 (0.05)	0.10 (0.01)	0.26 (0.06)	2.62 (0.53)	0.04 (0.01)	0.98 (0.20)
20	4.55 (1.17)	1.47 (0.05)	0.24 (0.02)	0.40 (0.09)	1.66 (0.34)	0.09 (0.03)	1.10 (0.23)
25	4.38 (0.62)	1.85 (0.11)	0.30 (0.02)	0.24 (0.05)	0.79 (0.17)	0.05 (0.01)	0.40 (0.09)
30	6.70 (1.38)	1.27 (0.04)	0.37 (0.02)	0.41 (0.09)	1.10 (0.23)	0.06 (0.02)	0.87 (0.18)
35	6.91 (1.80)	1.52 (0.10)	0.47 (0.03)	0.56 (0.13)	1.20 (0.26)	0.08 (0.03)	0.69 (0.15)
40	6.03 (0.46)	1.52 (0.03)	0.50 (0.02)	0.67 (0.14)	1.31 (0.27)	0.11 (0.03)	0.88 (0.18)
45	6.14 (0.75)	1.63 (0.10)	0.54 (0.03)	0.89 (0.19)	1.61 (0.34)	0.15 (0.04)	0.93 (0.20)
50	7.62 (0.55)	1.71 (0.04)	0.54 (0.01)	0.83 (0.17)	1.50 (0.31)	0.11 (0.02)	0.88 (0.18)
55	9.18 (0.75)	1.90 (0.14)	0.53 (0.02)	0.93 (0.20)	1.73 (0.37)	0.10 (0.03)	0.83 (0.18)
60	7.74 (1.86)	1.71 (0.06)	0.58 (0.07)	0.60 (0.14)	1.01 (0.21)	0.08 (0.03)	0.53 (0.11)
65	6.44 (0.93)	2.02 (0.16)	0.65 (0.04)	0.98 (0.22)	1.48 (0.32)	0.15 (0.04)	0.69 (0.15)
70	10.85 (1.08)	1.75 (0.06)	0.75 (0.05)	1.15 (0.25)	1.51 (0.31)	0.11 (0.03)	0.87 (0.18)
75	6.65 (1.05)	1.85 (0.16)	0.73 (0.05)	0.81 (0.18)	1.10 (0.24)	0.12 (0.03)	0.56 (0.12)
80	8.86 (1.38)	1.90 (0.07)	0.68 (0.03)	0.82 (0.17)	1.19 (0.25)	0.09 (0.02)	0.63 (0.13)
85	8.45 (1.58)	1.77 (0.17)	0.72 (0.05)	0.61 (0.14)	0.84 (0.18)	0.07 (0.02)	0.44 (0.10)
90	6.62 (0.71)	1.47 (0.05)	0.60 (0.03)	0.59 (0.13)	0.97 (0.20)	0.09 (0.02)	0.63 (0.13)
95	7.14 (1.23)	1.44 (0.12)	0.65 (0.05)	0.74 (0.17)	1.13 (0.24)	0.10 (0.03)	0.74 (0.16)
100	4.78 (1.06)	1.35 (0.11)	0.66 (0.07)	0.26 (0.06)	0.39 (0.08)	0.06 (0.02)	0.25 (0.05)
105	5.86 (0.91)	1.67 (0.13)	0.56 (0.04)	0.85 (0.19)	1.49 (0.32)	0.15 (0.04)	0.84 (0.18)
110	5.47 (0.58)	1.66 (0.07)	0.57 (0.02)	0.47 (0.10)	0.82 (0.17)	0.09 (0.02)	0.49 (0.10)
115	5.46 (0.58)	1.68 (0.09)	0.53 (0.03)	0.54 (0.11)	0.99 (0.20)	0.10 (0.02)	0.56 (0.12)
120	7.12 (1.05)	2.16 (0.12)	0.53 (0.03)	0.84 (0.22)	1.56 (0.32)	0.16 (0.05)	0.81 (0.17)
125	5.20 (0.51)	1.50 (0.07)	0.55 (0.03)	0.29 (0.06)	0.52 (0.11)	0.06 (0.01)	0.33 (0.07)
130	7.58 (1.29)	1.88 (0.09)	0.56 (0.02)	0.37 (0.08)	0.65 (0.13)	0.07 (0.02)	0.35 (0.07)
135	6.30 (0.92)	1.69 (0.08)	0.53 (0.03)	0.09 (0.02)	0.17 (0.04)	0.01 (0.00)	0.10 (0.02)

Table 7. As table 4, but for $E_{\text{in}} = 12.0$ eV.

θ (deg)	r	r'	r''	$5s[3/2]_2$ ($10^{-18} \text{ cm}^2 \text{ sr}^{-1}$)	$5s[3/2]_1$ ($10^{-18} \text{ cm}^2 \text{ sr}^{-1}$)	$5s'[3/2]_0$ ($10^{-18} \text{ cm}^2 \text{ sr}^{-1}$)	$5s'[1/2]_1$ ($10^{-18} \text{ cm}^2 \text{ sr}^{-1}$)
30	10.93 (7.00)	3.39 (0.64)	0.56 (0.10)	0.16 (0.04)	0.28 (0.06)	0.01 (0.01)	0.08 (0.02)
40	8.52 (2.19)	3.43 (0.44)	0.53 (0.04)	0.44 (0.10)	0.83 (0.17)	0.05 (0.02)	0.24 (0.05)
50	7.65 (3.49)	1.90 (0.18)	0.57 (0.03)	0.43 (0.09)	0.75 (0.16)	0.06 (0.03)	0.39 (0.08)
60	6.37 (1.73)	1.70 (0.11)	0.74 (0.05)	0.41 (0.09)	0.56 (0.12)	0.07 (0.02)	0.33 (0.07)
70	5.01 (1.68)	1.76 (0.20)	1.00 (0.07)	0.39 (0.09)	0.40 (0.08)	0.08 (0.03)	0.23 (0.05)
80	3.90 (0.74)	1.80 (0.12)	1.05 (0.06)	0.41 (0.09)	0.39 (0.08)	0.11 (0.03)	0.22 (0.05)
90	3.21 (0.43)	1.95 (0.07)	1.06 (0.03)	0.31 (0.06)	0.29 (0.06)	0.10 (0.02)	0.15 (0.03)
100	6.80 (3.06)	2.69 (0.31)	0.73 (0.05)	0.27 (0.06)	0.36 (0.08)	0.04 (0.02)	0.13 (0.03)
110	6.49 (1.40)	2.99 (0.21)	0.70 (0.05)	0.31 (0.07)	0.44 (0.09)	0.05 (0.02)	0.15 (0.03)
115	7.66 (3.00)	2.27 (0.23)	0.79 (0.05)	0.54 (0.11)	0.69 (0.14)	0.07 (0.02)	0.30 (0.06)
120	5.20 (1.30)	2.05 (0.30)	0.79 (0.08)	0.52 (0.12)	0.65 (0.14)	0.10 (0.03)	0.27 (0.06)
130	13.74 (5.89)	2.32 (0.13)	0.59 (0.13)	0.09 (0.03)	0.15 (0.03)	0.01 (0.00)	0.05 (0.01)

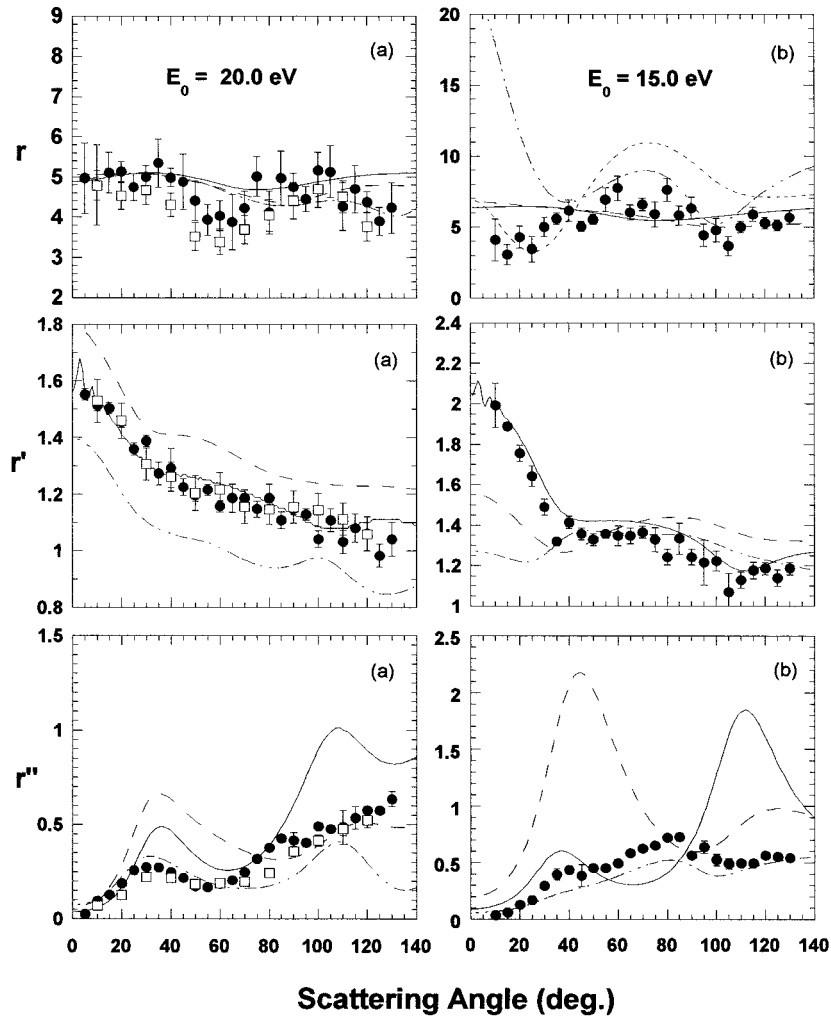


Figure 4. DCS ratios r , r' and r'' for incident energies of (a) 20.0 eV, (b) 15.0 eV, (c) 13.5 eV and (d) $E_0 = 12.0$ eV. Experiments: \bullet , present; \square , Khakoo *et al* (1994); \triangle , Phillips (1982). Theory: —, UFOMBT; (a) - - - -, RM31; (b) - - - -, RM31; - · - ·, RM31 (14.6 eV); (c) - · - ·, RM31; - - - -, RM15; - - - -, RM5; (d) - - - -, RM31; - · - ·, RM31 (11.90 eV); - - - -, RM31 (11.95 eV); - · - ·, RM31 (12.05 eV). Other theory: —, RDWA Zuo *et al* (1992). All data correspond to the incident energy labelled in the figures, unless stated otherwise. See text for discussion.

here that we observe (not shown in the graphs to avoid congestion) that r' moves closer to the experimental values as the number of coupled states is increased from 5 to 31. This indicates that the RM has not converged even for the 31-state expansion. The RDWA r' values are significantly higher than the experimental values. The possibility that this could be a problem (in the RDWA) due to the number of configurations used was eliminated when we examined this effect using our UFOMBT code. When we used a single configuration (equations (2)) we were still able to reproduce the 12-configuration UFOMBT results for r' to within 5%. We also note that the optical limit of r' (equation (3), RM: 0.84; UFOMBT: 1.12) is not realized.

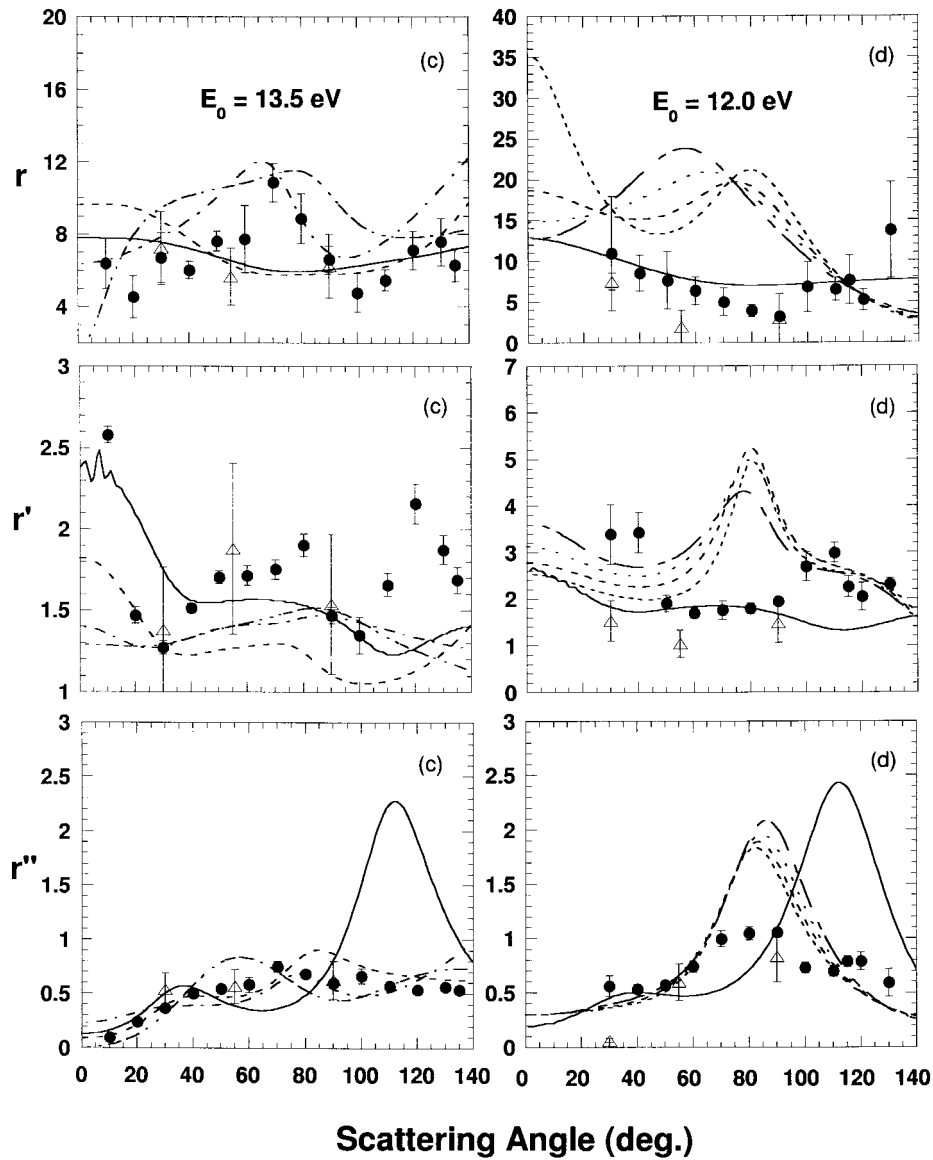


Figure 4. Continued.

This is possible evidence of the weak coupling of the core to the excited valence electron with r' approaching closely to the core statistical weight ratio at small momentum transfer—the core statistical weight ($= 2J_{\text{core}} + 1$) ratio for the levels in r' is 2:1. In fact, this is not fully realized, since the $\theta = 0^\circ$ limit of r' is close to 1.6, essentially halfway between the optical limit and the core statistical weight ratio.

For the ratio r'' (our most accurate DCS ratio) the experimental data (Khakoo *et al* 1994 and the present) show excellent agreement, except at 80° . All theories agree with the experimental data at some point, but not throughout the full angular range. The theories agree with each

other and with experiment at small angles, up to 15° for the RDWA, 25° for UFOMBT and up to 65° for the RM model. At large angles the experimental r'' values keep increasing, in accordance with the RDWA and the UFOMBT results. The UFOMBT in fact overestimates r'' by almost a factor of 2. However, the RM shows a decrease for r'' at larger angles. We note that the RM model does quantitatively better than the UFOMBT, but fails to describe the rising r'' values for $\theta > 110^\circ$.

4.1.2. $E_0 = 15.0$ eV For the 15.0 eV incident electron energy data (figure 4(b)), similar observations as at $E_0 = 20.0$ eV are reached in general. We note here that we again observe that the dependence of the RM on the number of states is more pronounced than at $E_0 = 20.0$ eV (this is not shown, again for the reasons of avoiding congestion in the graphs). The RM calculation shows a significant rise in r at low θ values, in complete opposition to the experimental values which are decreasing. Overall, for r , the UFOMBT and the RDWA perform similarly and show an average flat r value for all angles. However, these theories do not show the decrease in r at $\theta < 40^\circ$ as found in the experimental data. We show the RM31 r values at $E_0 = 14.6$ eV, and note the sensitive dependence of r on the value of incident electron energy.

For r' , the UFOMBT performs the best of all. The RM and the RDWA underestimate r' at $\theta < 40^\circ$. All the R-matrix calculations show major deviations from experiment at angles less than 40° . In the limiting case, the experimental value of r' in the limit of $\theta = 0^\circ$ is close to 2, i.e. the core statistical ratio. This perhaps shows an increased core–projectile electron interaction as compared to the $E_0 = 20.0$ eV case. For r'' the best agreement with experiment is found for the RM results, while the UFOMBT and RDWA are not even qualitatively in agreement with experiment.

4.1.3. $E_0 = 13.5$ eV The ratio results at $E_0 = 13.5$ eV are shown in figure 4(c). At this incident energy, which is 0.5 eV below the ionization threshold, we include the experimental results of Phillips (1982) at the limited angles of 30° , 55° and 90° . Agreement between the present experiment and Phillips' data is excellent. Below the ionization threshold, perturbative models, e.g. the UFOMBT, are not expected to be reliable, and here the UFOMBT shows an essentially flat behaviour with no structure for r . The RM calculations show greatly varying distributions of r for the 5-, 15- and 31-state calculations. Of these, the 31-state calculation gives some agreement with the experimental values. However, the RM-31 r value rises at small θ in contrast to the experimental results.

For r' , the UFOMBT and RM both are unable to reproduce the striking and complex undulating behaviour which shows minima at $\theta = 30^\circ$ and 100° and a sharp maximum at $\theta = 120^\circ$. The r' value rises very steeply from $\theta = 20^\circ$ to 10° . This ratio increases to a value greater than 2. The r'' behaviour is better reproduced by the 31-state RM results. The UFOMBT shows a very sharp maximum at around $\theta = 110^\circ$, contrary to experiment.

4.1.4. $E_0 = 12.0$ eV The figures appertaining to r , r' and r'' at this value are shown in figure 4(d). At this energy, DCSs are decreasing relative to those at higher E_0 values. With these reduced DCSs and correspondingly reduced scattered electron rates, data acquisition is slower. Thus data have only been acquired for a smaller range of scattering angles. The UFOMBT results are included despite the fact that this is not the regime of application for this model. We note that for r , UFOMBT results give better agreement with the experimental data, which shows a relatively smooth curve, displaying a shallow dip at $\theta = 90^\circ$. The observed r values are high, reaching a value of 12 at $\theta = 130^\circ$.

We observe very large values of r' at small scattering angles. There is significant disagreement with the results of Phillips (1982). Again the 31-state RM provides the best agreement with the present experiment. For r'' , we see good agreement with the results of Phillips (1982) except at $\theta = 30^\circ$. The RM results show qualitative agreement with the present experimental data, i.e. displaying the hump around $\theta = 90^\circ$. In the UFOMBT case, this hump is shifted to 120° . An interesting point here is that the models clearly show that r'' does not approach zero as θ tends to 0° , as is found at higher E_0 values. This means that at $\theta \approx 0^\circ$, there is significant spin exchange to excite the $5s[3/2]_2$ level from the ground level. At this energy, possibilities of resonance in the scattering were checked by carrying out the RM at $E_0 = 11.90, 11.95, 12.00$ and 12.05 eV. Despite the substantial changes seen in the RM31 results, particularly in the ratio r for incident energies around 12 eV, no evidence of resonances was found in the RM31 calculation in this region.

Finally we comment on the convergence of the RM at 15.0 eV and 13.5 eV (figures 4(b) and (c)), i.e., above and below the ionization potential by approximately 1 eV. We explicitly show the 5-, 15- and 31-state RM calculations in figure 4(c) while the 15 eV data have not been displayed for reasons of clarity. From these calculations, we observe that the change from being above the ionization continuum to below does not provide us with a more converged RM calculation. For example, for the 13.5 eV r and r' values, we observe significant variation between the various RM calculations. This picture suggests that a larger set of states needs to be incorporated into the RM before convergence will be obtained.

4.2. DCSs

The results of the absolute differential cross sections are presented in figures 5(a)–(d). The JPL results (Trajmar *et al* 1981) and the results of Phillips (1982) are also presented for comparison. For the RM model, only the results of the 31-state calculations are presented in figure 5.

4.2.1. $E_0 = 20.0$ eV At 20.0 eV incident energy (figure 5(a)), comparison of the present DCSs and those of Trajmar *et al* (1981) shows very good qualitative agreement, but in absolute comparison we observe that points with a factor of 2 difference occur, e.g., the DCSs for the $5s[3/2]_2$ at $\theta \approx 60^\circ$. The agreement between the present experimental results and the RM and RDWA results for the $J = 1$ transitions (which show typical forward-peaked dipole behaviour) is good. The UFOMBT shows good qualitative agreement, but does not do as well quantitatively. Considering the $J = 2$ and 0 levels, we observe poorer agreement than for the $J = 1$ levels. Whereas good agreement is observed at small angles, this situation becomes worse for scattering angles above 50° . An interesting point can be made when we consider the r' ratios and the corresponding DCSs. We see that for the $J = 1$ levels, the DCSs are well described by the RM, but the r' ratios are not described properly at all (see e.g., figure 4(a)). Comparison with the measurements of Filipovic *et al* (1988), which do not report error bars, shows that these measurements are too low by almost an order of magnitude.

4.2.2. $E_0 = 15.0$ eV At 15 eV the incident energy is 1 eV above the ionization potential and the theory must deal with the continuum. The metastable $J = 2$ and $J = 0$ level excitations show a behaviour which is different from those at $E_0 = 20.0$ eV, i.e., the DCSs become smaller as $\theta \rightarrow 0^\circ$. The RM calculations qualitatively show this behaviour especially for the $5s[1/2]_0$ level, but do not completely follow the experimental trend. The UFOMBT does not provide qualitative agreement for either metastable level. Both theories give good agreement with the experimental $J = 1$ DCSs at small θ . However, the RM also gives good agreement for large θ , whereas the UFOMBT does poorly here, indicating that it does not deal adequately with

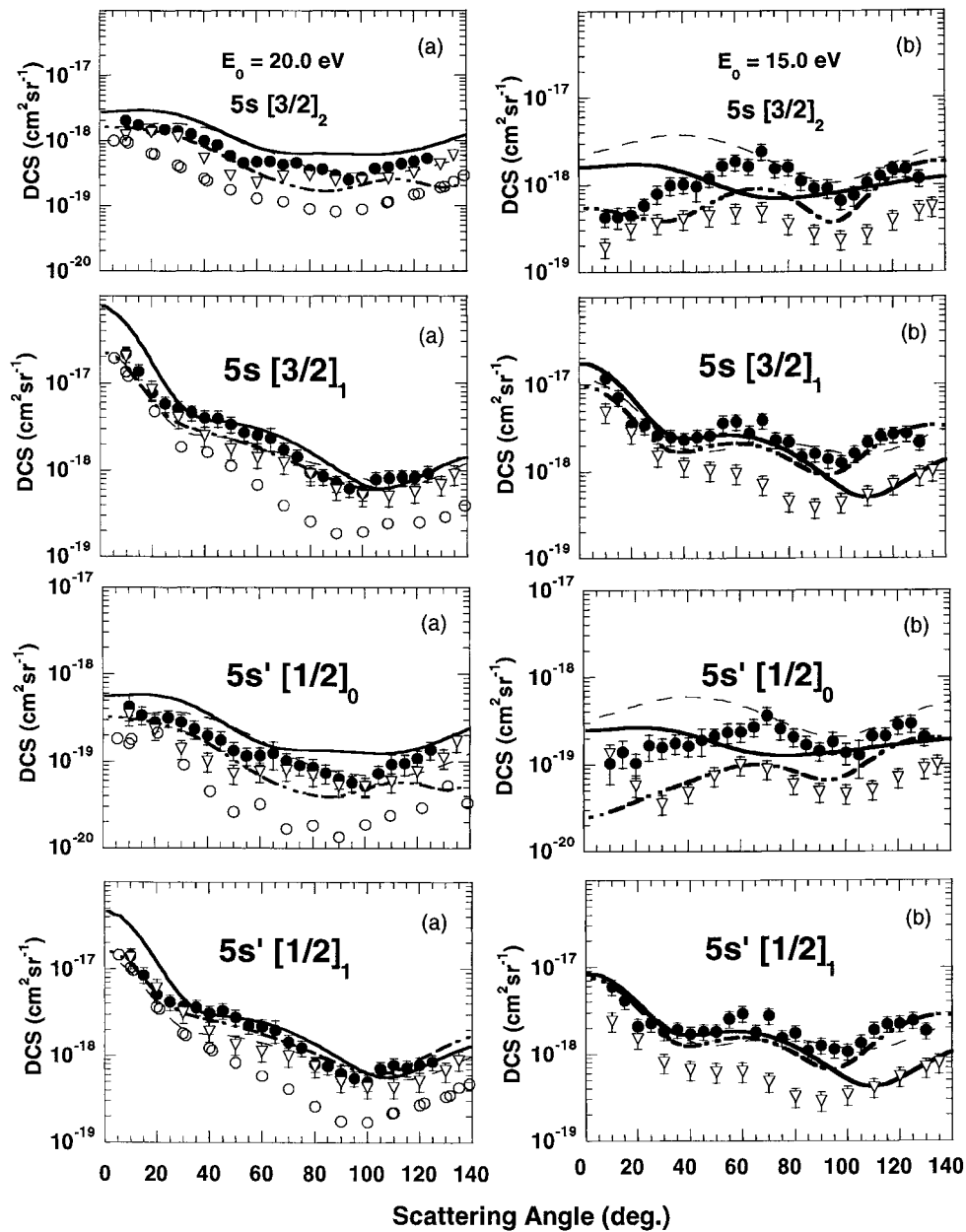


Figure 5. DCSs for electron-impact excitation of Kr for incident energies of (a) 20 eV, (b) 15 eV, (c) 13.5 eV and (d) 12.0 eV. Experiments: ●, Present; ▽, Trajmar *et al* (1981); ○, Filipovic *et al* (1988); △, Phillips (1982). Present theories: —, UFOMBT; ---, RM31 (a), (b); - · - ·, RM31 (c), (d). Other theory: — —, RDWA Zuo *et al* (1992). See text for discussion.

the exchange processes which dominate at large θ . However, we recall that the UFOMBT gives better r' values than the RM method. This r' problem will require fine tuning of the RM scheme. This observation also shows the importance of the DCS ratios in providing a fuller picture of the situation as regards testing recent models.

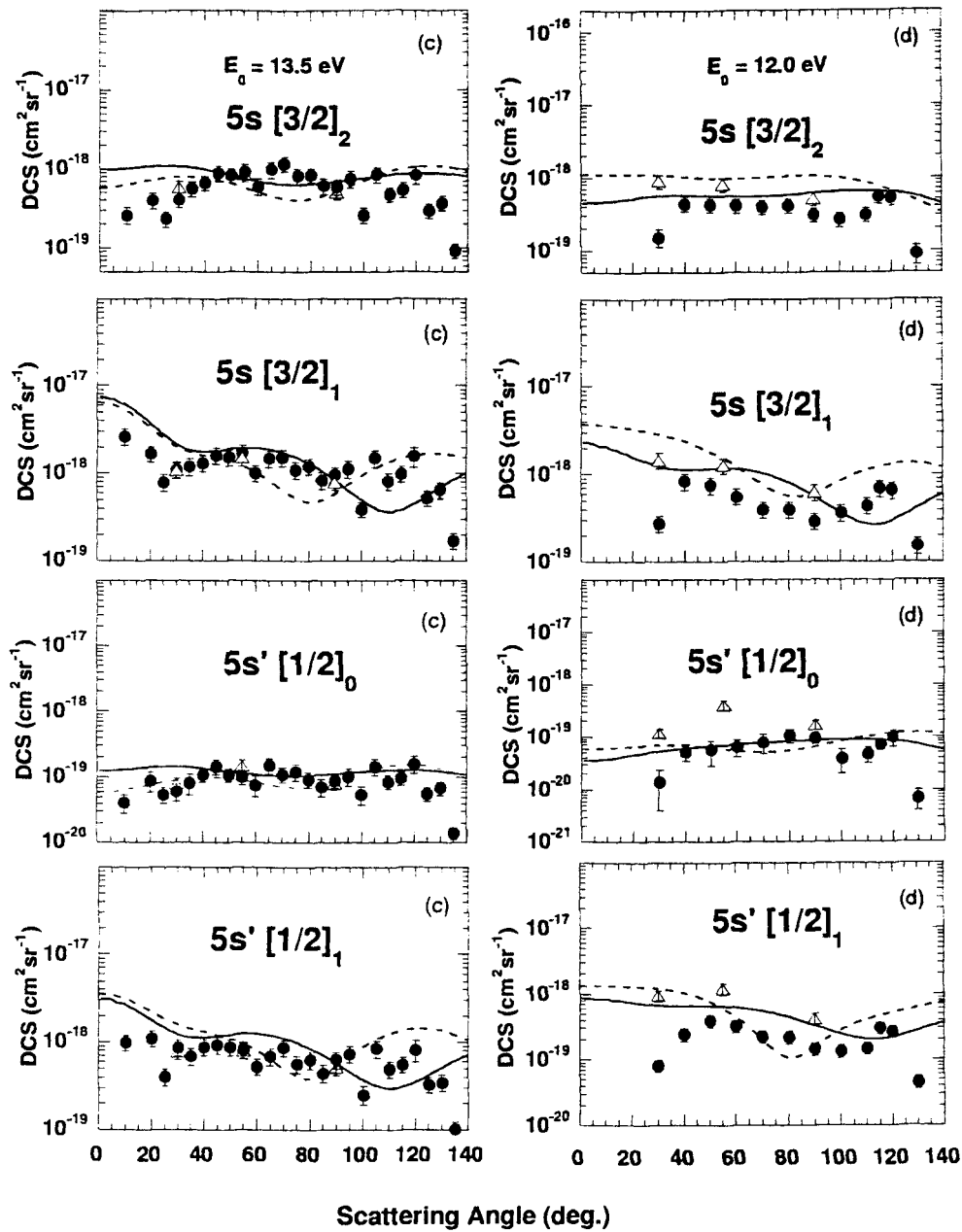


Figure 5. Continued.

The data from Trajmar *et al* (1981) are significantly lower than both our measured and calculated results for the entire range of θ . They are, however, in qualitative agreement with the present results. The major difference seems to be in the normalization procedure. We consider our measurements to be superior on account of our data analysis and normalization procedures, which have improved over this time period.

4.2.3. $E_0 = 13.5$ eV and 12.0 eV These energies are below the ionization potential and convergence of the expansion can be expected in the RM calculations. However, we see (figures 5(c), (d)) that agreement between the calculations and the experiment is not as good as at energies above the ionization threshold. At 13.5 eV, the experimental results of Phillips (1982) were obtained by scanning the incident electron energy for fixed angles of 30° , 55° and 90° . The agreement with our experimental results is good (figure 5(c)). In the angular range between 40° and 110° both calculations agree well in magnitude (on average) with the experiments, but differences in shape exist.

For the 12.0 eV incident energy, we could not obtain reliable experimental data at scattering angles below 30° due to large background signals. Also, measurements were made at 10° intervals instead of the previous 5° intervals because of the lower scattering rates observed and lower transmission efficiency at these low residual energies. The experimental results of Phillips (1982) are much higher, more than one order of magnitude in some instances, than our experimental results for the $5s'[1/2]$ case, but we agree better with the results of Phillips for the other cases (figure 5(d)). The theoretical calculations are much closer to our experimental results. As for 13.5 eV, the main differences between the calculations and the experiment remain at small angles ($\theta < 40^\circ$) and large angles ($\theta > 120^\circ$). One does not expect the UFOMBT to work in these ranges, and so any agreement with the UFOMBT is accidental. The RM does not provide good results here, as would be expected for the situation below the ionization potential.

4.3. Integral cross sections

The DCSs from the experimental data can be integrated over all solid angles to obtain integral cross sections (ICSs). However, since the present measurements do not cover all angles, these DCSs have to be extrapolated over large angles $\theta > 130^\circ$. An example of the extrapolation for $E_0 = 20$ eV and for the $5s[3/2]_2$ level is shown in figure 6. We can use the theoretical models as a guideline and from a spline fit to the data as well as this theory-guided extrapolation we have estimated integral cross sections for the excitation of the $4p^55s$ configuration levels at $E_0 = 20$ eV and 15 eV. Below these E_0 values the extrapolation become unreliable and has large ($> 50\%$) errors. These ICSs are given in table 8.

Comparisons with the available theoretical models UFOMBT and RM shows that at $E_0 = 20$ eV the UFOMBT produces ICSs that are consistently higher by approximately 50% than our experimental ICSs, whereas the RM produces ICSs that fall lower than the experimental values by about 30%. At $E_0 = 15$ eV, the models produce consistently lower ICSs than the experimental ones, but in very good agreement with experimental values.

Table 8. Integral cross sections for the electron-impact excitation of the $4p^55s$ configuration levels of Kr at $E_0 = 20$ eV and 15 eV. See text for details. ξ is the % of extrapolated part (130° – 180°) of the total integral cross section.

	20 eV				15 eV			
	$5s[3/2]_2$ (10^{-18} cm 2)	$5s[3/2]_1$ (10^{-18} cm 2)	$5s'[3/2]_0$ (10^{-18} cm 2)	$5s'[1/2]_1$ (10^{-18} cm 2)	$5s[3/2]_2$ (10^{-18} cm 2)	$5s[3/2]_1$ (10^{-18} cm 2)	$5s'[3/2]_0$ (10^{-18} cm 2)	$5s'[1/2]_1$ (10^{-18} cm 2)
Present experiment	8.0	28.5	1.85	22.3	14.2	29.2	2.43	21.7
Error (1 std)	2.55	6.59	0.666	5.17	2.01	4.45	0.347	3.19
ξ	32%	23%	36%	23%	14%	15%	14%	15%
UFOMBT	13.7	39.9	2.75	30.6	12.9	24.6	2.13	16.8
RM	5.36	22.8	1.13	21.9	10.8	26.4	1.33	20.7

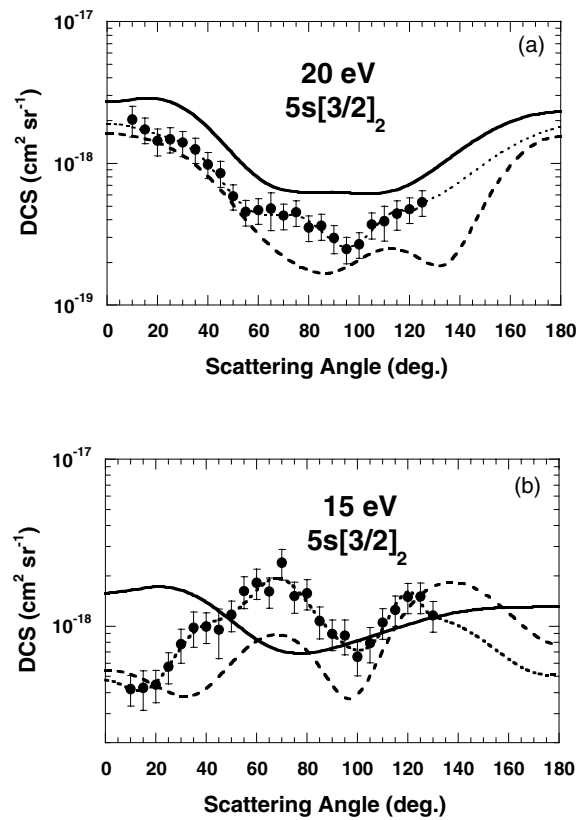


Figure 6. Determination of ICSs by extrapolation of the measured DCSs to large angles. The figures show the extent of the large-angle DCS contribution to the ICS and the extrapolation form (short-dashed curve) is determined using both theories as a guide. The legend is the same as figure 5.

5. Summary and conclusions

Although there remain significant differences between the experimental data and the R-matrix and UFOMBT calculations as far as ratios and DCSs are concerned, there are several points that we can make, as a result of comparison between the experimental measurements and the theoretical calculations in this work.

- (a) Considerable increases in the values of the ratios r and r' are found as the incident electron energy goes down from above to below the ionization threshold, which agrees in general with the predictions of both the R-matrix and UFOMBT models.
- (b) The DCS ratios of the R-matrix models at incident energies near the ionization threshold strongly depend on the number of states included in the calculation, but do not at energies far above the threshold, for example, at 20.0 eV.
- (c) From the RM results using a fine energy mesh, resonance effects on both the ratios and the DCSs at energies below the ionization threshold are not strong, and are thus as we expected according to our experimental results.
- (d) The experimental DCS ratios provide a new way of examining the data as well as a stringent test for theoretical models. The implication, in general, is that more work needs

to be done on the theoretical models to attain a better quantitative description of electron scattering by heavy noble gases.

- (e) This work also demonstrates that the DCS ratios are more sensitive than absolute DCSs to the adjustment of parameters included in the theoretical calculations. Therefore, measurement of the DCS ratios can be considered as a supplement to those of differential cross sections in testing theoretical scattering models and at the same time shedding new light on relativistic processes in the collision (Guo *et al* 1999).

Acknowledgments

This work was funded by the National Science Foundation under grant number NSF-RUI-PHY-9511549 (MAK), NSF-PHY-9605124 (VZ and KB) and NATO Scientific Collaboration Program under grant number CRG 950003 (AC and MAK). IK and ST gratefully acknowledge the support of the National Aeronautics and Space Administration. We thank Dr A D Stauffer for sending us the RDWA results in tabular form and Professor T J Gay for helpful discussions. The authors also want to thank Mr D Parsons, Mr H Fabris and Mr J Buell for their technical support and D Roundy for writing major portions of the spectrum fitting code used in this work.

References

- Abdallah J Jr, Clark R E H and Cowan R D 1988 *Los Alamos National Laboratory Manual* no LA-11436-M, vol I (unpublished)
- Allen L J, Brunger M J, McCarthy I E and Teubner P J O 1987 *J. Phys. B: At. Mol. Phys.* **20** 4861
- Bartschat K 1998 *Comput. Phys. Commun.* **114** 168
- Bartschat K, Hudson E T, Scott M P, Burke P G and Burke V M 1996 *Phys. Rev. A* **54** 998
- Bartschat K and Madison D H 1992 *J. Phys. B: At. Mol. Opt. Phys.* **25** 4619
- Becker K, Crowe A and McConkey J W 1992 *J. Phys. B: At. Mol. Opt. Phys.* **25** 3885
- Berrington K A, Eissner W and Norrington P H 1995 *Comput. Phys. Commun.* **92** 290
- Bray I 1994 *Phys. Rev. A* **49** 1066
- Bray I 1998 private communication
- Bray I and Stelbovics A T 1992 *Phys. Rev. A* **46** 6995
- Brunt J H, King G C and Read F H 1977 *J. Phys. B: At. Mol. Phys.* **10** 1289
- Clark R E H, Abdallah J Jr., Csanak G, Mann J B and Cowan R D 1988 *Los Alamos National Laboratory Manual* no LA-11436-M, vol II (unpublished)
- Cowan R D 1981 *The Theory of Atomic Structure and Spectra*, (Berkeley, CA: University of California Press)
- Danjo A 1988 *J. Phys. B: At. Mol. Opt. Phys.* **21** 3759
- 1989 *J. Phys. B: At. Mol. Opt. Phys.* **22** 951
- Dümmler M, Hanne G F and J Kessler J 1995 *J. Phys. B: At. Mol. Opt. Phys.* **28** 2985
- Filipovic D 1988 *PhD Thesis* University of Belgrade
- Filipovic D, Marinkovic B, Pejcev V and Vuskovic L 1988 *Fizika* **20** 421
- Fontes C J 1998 *J. Phys. B: At. Mol. Opt. Phys.* **31** 175
- Furst J E, Wijayaratra W M K P, Madison D H and Gay T J 1993 *Phys. Rev. A* **47** 3775
- Guo X, Khakoo M A, Mathews D F, Mikaelian G, Crowe A, Kanik I, Trajmar S, Zeman V, Bartschat K and Fontes C J 1999 *J. Phys. B: At. Mol. Opt. Phys.* **32** L155
- Hibbert A 1975 *Comput. Phys. Commun.* **9** 141
- Kaur S, Srivastava R, McEachran R P and Stauffer A D 1998 *J. Phys. B: At. Mol. Opt. Phys.* **31** 4833
- Khakoo M A, Beckmann C E, Trajmar S and Csanak G 1994 *J. Phys. B: At. Mol. Opt. Phys.* **27** 3159
- Khakoo M A, Trajmar S, LeClair L R, Kanik I, Csanak G and Fontes C J 1996a *J. Phys. B: At. Mol. Opt. Phys.* **29** 3455
- Khakoo M A, Trajmar S, S. Wang, Kanik I, Aguirre A, Fontes C J, Clark R E H and Abdallah Jr. J 1996b *J. Phys. B: At. Mol. Opt. Phys.* **29** 3477
- Khakoo M A, Tran T D, Bordelon D and Csanak G 1992 *Phys. Rev. A* **45** 219
- Kuhn H G 1962 *Atomic Spectra* (New York: Academic)

- McClelland J J, Kelley M H and Celotta R J 1989 *Phys. Rev. A* **40** 2321
- Moore C E 1952 *Atomic Energy Levels* NBS Circular no 467 (Washington, DC: US Govt Printing Office)
- Nakazaki S, Berrington K A, Eissner W B and Itikawa Y 1997 *J. Phys. B: At. Mol. Opt. Phys.* **30** 5805
- Nickel J C, Zetner P W, Shen G and Trajmar S 1989 *J. Phys. E: Sci. Instrum.* **22** 730
- Norén C, Karras W L, McConkey J W and Hammond P 1996 *Phys. Rev. A* **54** 510
- Norén C and McConkey J W 1996 *Phys. Rev. A* **53** 1559
- Phillips J M 1982 *J. Phys. B: At. Mol. Phys.* **15** 4259
- Pichou F, Huetz A, Joyez G and Landau M 1978 *J. Phys. B: At. Mol. Phys.* **11** 3683
- Register D F, Trajmar S and Srivastava S K 1980 *Phys. Rev. A* **21** 1134
- Rhodes C K 1983 *Excimer Lasers (Topics in Applied Physics)* 2nd enlarged edn (New York: Springer)
- Scholten R E, Shen G F and Teubner P J O 1993 *J. Phys. B: At. Mol. Opt. Phys.* **26** 987
- Srivastava S K, Tanaka H, Chutjian A and Trajmar S 1981 *Phys. Rev. A* **23** 1134
- Stockman K A, Karaganov V, Bray I and Teubner P J O 1999 *J. Phys. B: At. Mol. Opt. Phys.* **32** 3003
- Tawara H and Phaneuf R A 1988 *Comment. At. Mol. Phys.* **21** 177
- Trajmar S, Kanik I, Khakoo M A, LeClair L, Bray I, Fursa D V and Csanak G 1999 *J. Phys. B: At. Mol. Opt. Phys.* **32** 2801
- Trajmar S, Srivastava S K, Tanaka H and Nishimura H 1981 *Phys. Rev. A* **23** 2167
- Veerasingham R *et al* 1995 *48th Gaseous Electronics Conf. Bull. Am. Phys. Soc.* **40** 1583
- Williamson W, Drallos P J and Nagorny V P 1994 *Proc.SPIE* **2174** 163
- Yu D H, Hayes P A, Furst J E, and Williams J F 1997a, *Phys. Rev. Lett.* **78** 2724
- Yu D H, Hayes P A, Williams J F, and Furst J E 1997b, *J. Phys. B: At. Mol. Opt. Phys.* **30** 1799
- Zeman V and Bartschat K 1997 *J. Phys. B: At. Mol. Opt. Phys.* **30** 4609
- Zeman V, Bartschat K, Gay T J and Trantham K W 1998a *Phys. Rev. Lett.* **79** 1825
- Zeman V, Bartschat K, Noren C and McConkey J W 1998b *Phys. Rev. A* **58** 1275
- Zuo T, McEachran R P and Stauffer A D 1992 *J. Phys. B: At. Mol. Opt. Phys.* **25** 3393